MOTION BLUR KERNEL ESTIMATION VIA SALIENT EDGES AND LOW RANK PRIOR

Jinshan Pan[†], Risheng Liu[‡♯§], Zhixun Su[†], and Guili Liu[†♭]

[†] School of Mathematical Sciences, Dalian University of Technology, China
[‡] School of Software Technology, Dalian University of Technology, China
[♭] Basic Teaching and Research Department, Harbin Finance University, China
[♯] State Key Laboratory of Novel Software Technology, Nanjing University, China
[§] Faculty of Electronic Information and Electrical Engineering, Dalian University of Technology, China

ABSTRACT

Blind image deblurring, i.e., estimating a blur kernel from a single input blurred image is a severely ill-posed problem. In this paper, we show how to effectively apply low rank prior to blind image deblurring and then propose a new algorithm which combines salient edges and low rank prior. Salient edges provide reliable edge information for kernel estimation, while low rank prior provides data-authentic priors for the latent image. When estimating the kernel, the salient edges are extracted from an intermediate latent image solved by combining the predicted edges and low rank prior, which help preserve more useful edges than previous deconvolution methods do. By solving the blind image deblurring problem in this fashion, high-quality blur kernels can be obtained. Extensive experiments testify to the superiority of the proposed method over state-of-the-art algorithms, both qualitatively and quantitatively.

Index Terms— Blind image deblurring, low rank prior, salient edges, kernel estimation, image restoration

1. INTRODUCTION

Blind image deblurring has gained considerable attention and achieved great success in recent years. The formation process of image blur is usually modeled as:

$$B = I * k + \varepsilon, \qquad (1)$$

where B, I, k and ε represent the blurred image, latent image, blur kernel, and the additive noise, respectively. $*$ denotes the convolution operator. It is a well-known ill-posed inverse problem, which requires regularization in order to obtain a high quality latent image.

1.1. Related Work

In order to make blind deblurring more tractable, early approaches imposed constraints on motion blur kernels [1, 2],

and the solutions can be usually obtained by maximum a posterior (MAP) approach.

Recently, Fergus et al. [3] proposed a zero-mean Mixture of Gaussian to fit the distribution of natural image gradients. Levin et al. [4, 5] proposed a hyper-Laplacian prior to fit the distribution of natural image gradients. However, because naive MAP inference could fail on natural images, they maximized marginalized distributions to get a better solution.

Another group of methods still followed the line of altering the naive MAP framework to estimate the blur kernels. To avoid and overcome the naive limitations of MAP, a variety of strategies have been proposed. Shan et al. [6] used a certain parametric model to approximate the heavy-tailed natural image prior. Moreover, to avoid the delta kernel solution, they used a large regularization weight to suppress insignificant structures and preserve strong ones. Krishnan et al. [7] proposed a normalized sparsity prior, i.e., ℓ_1/ℓ_2 regularizer. This new regularizer favors latent images over blurred ones. Joshi et al. [8] and Cho et al. [9] directly restored sharp edges from blurred images and relied on them to estimate blur kernels. The works [10, 11, 12] employed shock filter to predict the sharp edges for kernel estimation. Cho and Lee [10] performed bilateral filter and edge thresholding at each iteration to preserve the sharp edges. The kernel estimation process was achieved by a coarse-to-fine strategy. Xu and Jia [11] extended the sharp edges selection method [10] and selected the large scale edges for kernel estimation. Pan et al. [12] went a further step. They proposed an adaptive edge selection method and an effective gradient constraint for kernel estimation. Sun et al. [13] employed patch priors to restore useful edges for kernel estimation. These schemes have been extensively validated in blind image deblurring. To avoid ad-hoc edge selection step, Xu et al. [14] and Pan and Su [15] proposed ℓ_0-regularized kernel estimation. Due to the properties of ℓ_0-norm, these methods are able to select large scale edges for kernel estimation.

Sparse representation as a new powerful image prior has also been employed in blind deblurring [16, 17, 18]. Because sparse representation is able to provide data-authentic priors

in the kernel estimation, these methods have also achieved state-of-the-art results.

1.2. Our Contribution

In this paper, we find that although the sharp edges are able to help kernel estimation, if the priors imposed on the intermediate latent images are improper, the accuracy of kernel estimates are still affected by the salient edges extracted from intermediate latent images. Based on above analysis, we in this paper propose a robust motion blur kernel estimation method via salient edges and low rank prior. Salient edges are able to avoid the delta kernels, while the low rank prior used in the intermediate latent image restoration can provide more useful data for the kernel estimation. Although low rank prior has been successfully applied to many computer vision problems, to the best of our knowledge, few algorithms utilize low rank prior for kernel estimation.

2. KERNEL ESTIMATION VIA SALIENT EDGES AND LOW RANK PRIOR

The proposed kernel estimation is based on the improved MAP framework. It is achieved by iteratively solving latent image restoration (Section 2.1) and kernel estimation (Section 2.2).

2.1. Intermediate Latent Image Restoration via Low Rank Prior

Intermediate latent image restoration plays a critical role in kernel estimation process, because it provides data when estimating blur kernels. In this section, we will propose a new robust intermediate latent image estimation method.

Sparse representation and nonlocal self-similarity have been successfully used for image restoration problems. In these methods, images are often decomposed into small patches to better fit the sparse representation assumption [19] or generate the weights by nonlocal neighboring patches [20]. The works [21, 22] provided the connection among the sparse representation, nonlocal self-similarity, and low rank approximation. Moreover, Dong et al. [21] proposed the following model to remove the noise in the image:

$$\min_{X} \|Y - X\|_F^2 + \lambda \|X\|_*, \qquad (2)$$

where $Y = [y_1, y_2, \ldots, y_N] \in \mathbb{R}^{n \times N}$ is a set of similar image patches with noise, X denotes the restored image patches without noise, and $\|X\|_*$ denotes the nuclear norm of X, i.e., the sum of the singular values of the matrix X. Model (2) is very effective in image denoising [21].

Inspired by the work [21], we employ the low rank prior to guide the intermediate latent image restoration. Our restoration model is defined as

$$\min_{I,L} \|I * k - B\|_2^2 + \beta \|\nabla I - \nabla S\|_2^2 + \tau LR(I, L), \qquad (3)$$

where $\nabla I = (\partial_x I, \partial_y I)^T$ is the gradient of the image I, ∇S is the salient edges to be detailed in Section 2.2, and $LR(I, L)$
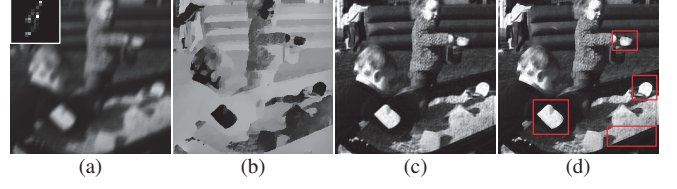

Fig. 1. The effectiveness of the proposed intermediate latent image restoration model (3). (a) Blurred image and kernel. (b) ∇S map visualized using Poisson reconstruction. (c) Result without the second term in model (3). (d) Result with model (3). The red boxes shown in (d) contains some sharp edges.

is defined as

$$LR(I, L) = \sum_i \|R_i I - L_i\|_F^2 + \lambda \|L_i\|_*, \qquad (4)$$

where L_i denotes the restored image patches with low rank property and $R_i I = [I_{i_1}, I_{i_2}, \ldots, I_{i_N}] \in \mathbb{R}^{n \times N}$ is the i-th set of similar image patches extracted from the image I, which can be obtained by k-Nearest-Neighbor method according to [21]. We explain each term of model (3) in detail as follows.

1. The first term is the reconstruction error constraint which ensures the recovered image should be consistent with the input image with respect to the estimated degradation model.

2. The second term encourages the gradient of I to be similar to the salient edges ∇S, which is able to preserve sharp edges in the recovered latent image.

3. The third term uses low rank prior to provide a data-authentic prior for the latent image.

Discussion: It is noted that the works [21, 22] also employed low rank prior to restore images. However, our model is different from [21, 22]. Our goal is mainly to recover the sharp edges. Thus, the edge-preserving term (i.e., the second term in model (3)) is used. This is the main difference from [21, 22].

Figure 1 shows comparison results which demonstrate the effectiveness of our model (3). We note that our estimated result shown in Figure 1(d) contains more sharp edges which will provide more useful data for kernel estimation.

2.2. Kernel Estimation via Salient Edges

In order to avoid the delta kernel solution and get a better kernel estimate, most iterative deblurring methods [10, 11] are carefully designed to select sharp edges for kernel estimation. Recent work [12] proposes an edge selection method based on an adaptive Total Variation (TV) model, which has been proven to be effective in practice. To increase the robustness of kernel estimation, we adopt the edge selection method [12] to select the salient edges for kernel estimation. The computation is as follows.

First, we extract the main structures from the intermediate image I by

$$\min_{I_s} \sum_{\mathbf{x}} \|\nabla I_s(\mathbf{x})\|_2 + \frac{1}{2\theta\omega(\mathbf{x})}(I_s(\mathbf{x}) - I(\mathbf{x}))^2, \quad (5)$$

where $\omega(\mathbf{x}) = \exp(-(r(\mathbf{x}))^{0.8})$ and $r(\mathbf{x})$ is defined as

$$r(\mathbf{x}) = \frac{\|\sum_{\mathbf{y} \in \mathfrak{N}_h(\mathbf{x})} \nabla B(\mathbf{y})\|_2}{\sum_{\mathbf{y} \in \mathfrak{N}_h(\mathbf{x})} \|\nabla B(\mathbf{y})\|_2 + 0.5}, \quad (6)$$

in which $\mathfrak{N}_h(\mathbf{x})$ is an $h \times h$ window centered at pixel $\mathbf{x}$.

Second, we compute an image $\tilde{I}_s$ by a shock filter [23]:

$$\frac{\partial \tilde{I}_s}{\partial t} = -\text{sign}(\triangle \tilde{I}_s)\|\nabla \tilde{I}_s\|_2,$$
$$\tilde{I}_s|_{t=0} = I_s, \quad (7)$$

Finally, the salient edges which are used for kernel estimation can be obtained by

$$\nabla S = \nabla \tilde{I}_s \odot H(\|\nabla \tilde{I}_s\|_2, t), \quad (8)$$

where $\odot$ denotes the pixel-wise multiplication operator, t is a threshold, and $H(\|\nabla \tilde{I}_s\|_2, t)$ is defined as

$$H(\nabla \tilde{I}_s, t) = \begin{cases} 1, & \|\nabla \tilde{I}_s\|_2 \geqslant t, \\ 0, & \text{otherwise.} \end{cases} \quad (9)$$

Based on the above considerations, our kernel estimation model is defined as

$$\min_{k} \|\nabla S * k - \nabla B\|_2^2 + \gamma\|k\|_2^2,$$
$$\text{s.t.} \quad k(\mathbf{x}) \geq 0, \quad \sum_{\mathbf{x}} k(\mathbf{x}) = 1. \quad (10)$$

3. OPTIMIZATION

In this section, we provide more details on solving intermediate latent image estimation model (3) and kernel estimation model (10).

3.1. Optimization for Intermediate Latent Image Restoration

Minimizing model (3) involves simultaneously computing two variables: I and L, which is computationally challenging. We employ the alternating minimization scheme, which is widely adopted when dealing with multiple optimization variables. Following this optimization framework, we address each of the optimization variable separately and present an overall efficient optimization algorithm.

3.1.1. Intermediate latent image I updating

With L fixed, the problem for updating intermediate latent image I is as

$$\min_{I} \|I * k - B\|_2^2 + \beta\|\nabla I - \nabla S\|_2^2 + \tau \sum_{i} \|R_i I - L_i\|_2^2. \quad (11)$$

It is a least squared problem and its closed form solution can be obtained by using Fast Fourier Transform (FFT):

$$I = \mathcal{F}^{-1}\left(\frac{\overline{\mathcal{F}(k)}\mathcal{F}(B) + \beta F_2 + \tau\mathcal{F}(\sum_i R_i^T L_i)}{\overline{\mathcal{F}(k)}\mathcal{F}(k) + \beta F_1 + \tau\mathcal{F}(\sum_i R_i^T R_i)}\right), \quad (12)$$

where $\mathcal{F}(\cdot)$ and $\mathcal{F}^{-1}(\cdot)$ denote the FFT and inverse FFT, respectively, $\overline{\mathcal{F}(\cdot)}$ is the complex conjugate operator, $F_1 = \overline{\mathcal{F}(\partial_x)}\mathcal{F}(\partial_x) + \overline{\mathcal{F}(\partial_y)}\mathcal{F}(\partial_y)$, and $F_2 = \overline{\mathcal{F}(\partial_x)}\mathcal{F}(\partial_x S) + \overline{\mathcal{F}(\partial_y)}\mathcal{F}(\partial_y S)$.

3.1.2. Low rank part L updating

With I fixed, the problem for updating L is

$$\min_{L} \tau \sum_{i} \|R_i I - L_i\|_F^2 + \lambda\|L_i\|_*, \quad (13)$$

which is a standard low-rank approximation problem [24]. Thus, its closed form solution can be obtained by

$$L_i = U_i \mathcal{S}_{\lambda/(2\tau)}[\Sigma_i]V_i^T, \quad (14)$$

where $U_i\Sigma_i V_i^T$ is the SVD of $R_i I$ and $\mathcal{S}_{\lambda/(2\tau)}[x]$ is defined as

$$\mathcal{S}_{\lambda/(2\tau)}[x] = \begin{cases} x - \lambda/(2\tau), & x > \lambda/(2\tau), \\ x + \lambda/(2\tau), & x < -\lambda/(2\tau), \\ 0, & \text{otherwise.} \end{cases} \quad (15)$$

To increase the accuracy of L, we adopt the similar strategy proposed by [21] to estimate L.

Based on above analysis, our alternating minimization algorithm for the intermediate latent image restoration is summarized in Algorithm 1.

Algorithm 1 Intermediate Latent Image Restoration

Input: Blur image B, blur kernel k, and salient edges ∇S
$I \leftarrow B$.
for $i = 1 \rightarrow 3$ **do**
    Estimate L according to (13).
    Estimate I according to (11).
end for
Output: Intermediate latent image I.

3.2. Optimization for Kernel Estimation

By writing convolution as matrix multiplication, model (10) can be written as

$$\min_{V_k} V_k^T(A_x^T A_x + A_y^T A_y + \gamma)V_k - 2(A_x^T V_{Bx} + A_y^T V_{By})^T V_k,$$
$$\text{s.t.} \quad V_k \succeq 0, \mathbf{1}^T V_k = 1, \quad (16)$$

where A_x and A_y denote the Toeplitz matrices form of $\partial_x S$ and $\partial_y S$ w.r.t k, respectively. V_{Bx}, V_{By}, and V_k denote the vector form of $\partial_x B$, $\partial_y B$, and k, respectively. $\mathbf{1}^T = [1, 1, \ldots, 1]$ has the same size to V_k. Note that model (16) is a quadratic programming. Thus, the global solution can be obtained. We employ the dual active-set method to solve model (16).

Finally, to increase the accuracy of kernel estimation, we adopt the iterative coarse-to-fine optimization framework that is commonly used in recent methods [10, 11, 12, 14, 13]. Algorithm 2 presents the main steps in one image level.

Algorithm 2 The Proposed Kernel Estimation Algorithm

Input: Blur image B.

Initialize I and k from the previous coarser level.

for $j = 1 \to 5$ (iterations at each level) **do**

  Compute ∇S according to (8).

  Estimate k according to (16).

  Estimate I by Algorithm 1.

  Decrease the values of θ and t to include more edges for kernel estimation.

end for

Output: Blur kernel k.

---

4. FINAL LATENT IMAGE RESTORATION

The computed intermediate latent image is not the final latent natural image estimate due to lack of details (see Figure 1 (d)). To obtain a better latent image with finer textures, we in this paper choose the non-blind deblurring method with a hyper-Laplacian prior [25] to recover the final latent image, which is defined as

$$\min_I \|I * k - B\|_2^2 + \lambda_f(\|\partial_x I\|^{0.8} + \|\partial_y I\|^{0.8}). \quad (17)$$

We empirically set $\lambda_f = 3e^{-3}$ in our experiments.

5. ANALYSIS ON THE LOW RANK PRIOR IN KERNEL ESTIMATION

Although many previous approaches (e.g., [10, 11, 12]) mainly focus on extracting salient edges from the intermediate latent image for kernel estimation, we note that if the intermediate latent image cannot be recovered well, the salient edges will have detrimental effect on the kernel estimation. To demonstrate the effectiveness of low rank prior in the kernel estimation, we compare the proposed method with the commonly used anisotropic TV regularizer that is employed in [12] and the proposed method without low rank prior (i.e., setting $\tau = 0$ in (3)) under the same salient edges selection strategy. We use the synthetic dataset from [4], which contains 8 blur kernels and 32 blurred images, for comparison.

In Figure 2(a), we plot the cumulative histograms of deconvolution error ratios in the same way as [4]. We note that image deblurring without low rank prior is less effective (see the baby blue bar in Figure 2(a)). On the other hand, image deblurring with commonly used anisotropic TV method [12] is still not effective. The comparison results show that low rank prior is able to provide reliable data for kernel estimation, thereby facilitating kernel estimation. In Figure 2(b), we choose an example (i.e., the "im02_ker01" test case in the dataset in [4]) to demonstrate the validity of our kernel estimation algorithm. Sum of Squared Differences Error (SSDE) is employed to measure the quality of kernel estimates at each iteration. As can be seen from Figure 2(b), the estimation error for the blur kernel is decreasing with increasing iterations, which empirically justifies the effectiveness of the proposed Algorithm 2. Moreover, the proposed method performs better at each iteration.
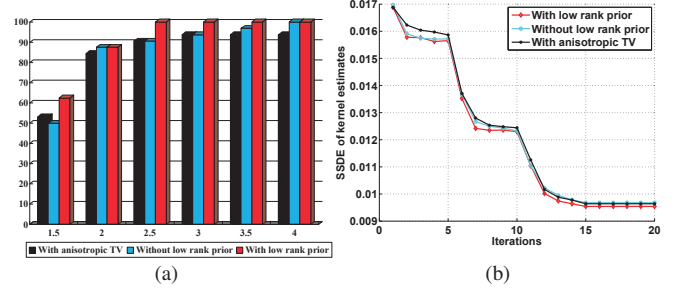

Fig. 2. The effectiveness of low rank prior in kernel estimation. (a) Quantitative comparison by using cumulative histograms of error ratios. (b) Kernel estimation error plot in terms of SSDE at each iteration.

6. EXPERIMENTAL RESULTS

In this section, we conduct extensive evaluations on the proposed approach. The parameter t determines the number of salient edges used for kernel estimation, we in this paper adaptively set its initial value according to [10]. The parameters β, τ, γ, and θ are empirically set to be $5e^{-5}$, $1e^{-2}$, $1e^{-2}$, and 1, respectively. The choice of these values are based on the extensive experimental results. The parameter λ is chosen according to [21]. In the kernel estimation, all color images are converted to grayscale ones. In the final deconvolution process, each color channel is separately processed. Our unoptimized MATLAB implementation takes several minutes to estimate a 25×25 kernel from a 255×255 image with an Intel Xeon CPU@2.53GHz and 12GB RAM.

Quantitative Evaluation on the Dataset of [4]: We perform quantitative evaluation of our method using the data set from [4]. For evaluation with each test case, we follow the method used in [4]. We also use the provided script and non-blind deconvolution function to generate the results, for fairness. The error ratio proposed by [4] is used to measure the quality of estimated results. We compare our method with those of Fergus et al. [3], Shan et al. [6], Cho and Lee [10], Xu and Jia [11], Levin et al. [5], Krishnan et al. [7], Pan et al. [12], Xu et al. [14], Zhong et al. [26], and Sun et al. [13]. The comparison results are shown in Figure 3. As indicated in [4], error ratios over 2 will make the result visually implausible. One can see that our method performs the best and all the error ratio values are below 3. This demonstrates the effectiveness of the proposed method.

Figure 4 shows one example from the test dataset. As can be seen from Figure 4, methods of Shan et al. [6], Cho and Lee [10], Krishnan et al. [7], Pan et al. [12], Zhong et al. [26] fail to provide reasonable kernel estimates. The deblurred results contain some obvious blur. The kernel estimates of [11, 14] look better, but the corresponding kernel similarity values are lower than that of our method. In contrast, the result of our method has the best visual quality. Moreover, the highest kernel similarity value also shows that the proposed kernel estimation method outperforms other state-of-the-art methods.
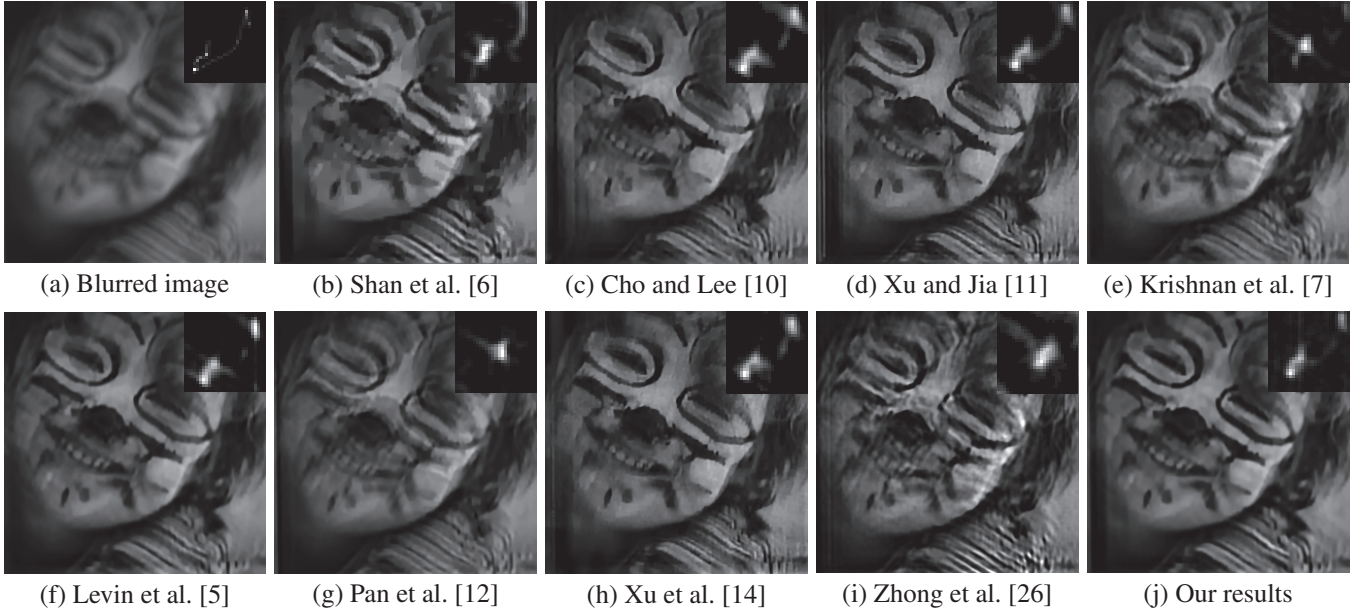
(a) Blurred image   (b) Shan et al. [6]   (c) Cho and Lee [10]   (d) Xu and Jia [11]   (e) Krishnan et al. [7]

(f) Levin et al. [5]   (g) Pan et al. [12]   (h) Xu et al. [14]   (i) Zhong et al. [26]   (j) Our results

Fig. 4. Comparison with state-of-the-art methods on a synthetic example. The kernel similarity values in (b)-(j) are 0.5811, 0.4503, 0.6328, 0.5142, 0.6179, 0.4110, 0.6225, 0.4341, and 0.6504, respectively.
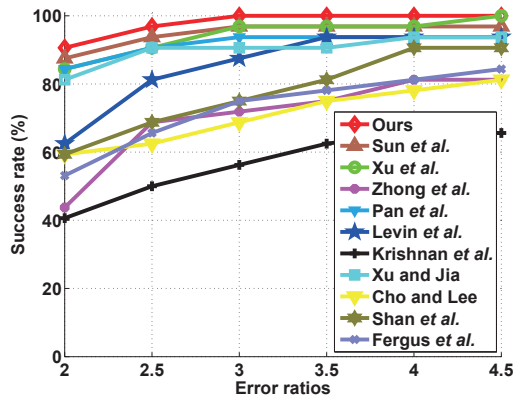

Fig. 3. Quantitative comparison with state-of-the-art methods on the dataset [4]. Our method performs the best.

Evaluation on Real Blurred Images: Now we test our method with some real blurred images. Figure 5 shows an example that is also presented in [11]. The deblurred results of [6, 10, 11, 7, 5] still contain some blur. The deblurred result of Zhong et al. [7] contains some obvious ringing artifacts. However, the deblurred result from the proposed method contains clearer and finer textures than that of [12] in the red boxes. More experimental results are included in the supplemental material.

7. CONCLUSIONS

In this work, we have presented an effective method for blind image deblurring. The proposed method combines salient edges and low rank prior. The salient edges provide reliable edge information, while the low rank prior offers faithful priors for the latent image. Their combination greatly improves

the quality of kernel estimation. Both quantitative and qualitative evaluations on challenging examples demonstrate that the proposed method performs favorably against several state-of-the-art algorithms.

8. REFERENCES

[1] T. Chan and C. Wong, "Total variation blind deconvolution," *IEEE Transactions on Image Processing*, vol. 7, no. 3, pp. 370–375, 1998.

[2] Y.-L. You and M. Kaveh, "Blind image restoration by anisotropic regularization," *IEEE Transactions on Image Processing*, vol. 8, no. 3, pp. 396–407, 1999.

[3] R. Fergus, B. Singh, A. Hertzmann, S. T. Roweis, and W. T. Freeman, "Removing camera shake from a single photograph," *ACM Trans. Graph.*, vol. 25, no. 3, pp. 787–794, 2006.

[4] A. Levin, Y. Weiss, F. Durand, and W. T. Freeman, "Understanding and evaluating blind deconvolution algorithms," in *CVPR*, 2009, pp. 1964–1971.

[5] A. Levin, Y. Weiss, F. Durand, and W. T. Freeman, "Efficient marginal likelihood optimization in blind deconvolution," in *CVPR*, 2011, pp. 2657–2664.

[6] Q. Shan, J. Jia, and A. Agarwala, "High-quality motion deblurring from a single image," *ACM Trans. Graph.*, vol. 27, no. 3, pp. 73, 2008.
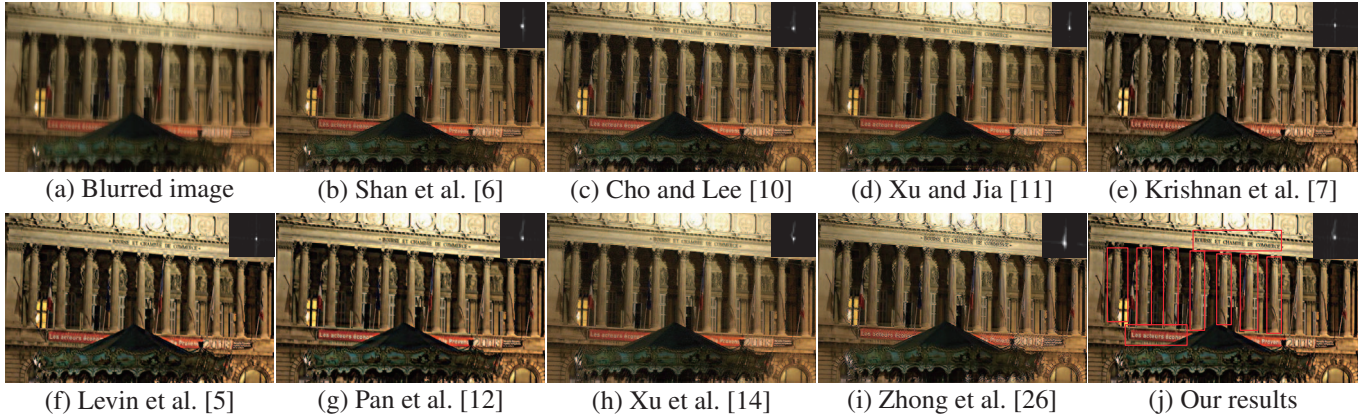
| (a) Blurred image | (b) Shan et al. [6] | (c) Cho and Lee [10] | (d) Xu and Jia [11] | (e) Krishnan et al. [7] |
| (f) Levin et al. [5] | (g) Pan et al. [12] | (h) Xu et al. [14] | (i) Zhong et al. [26] | (j) Our results |

Fig. 5. Comparison with state-of-the-art methods on a real captured example. The size of our estimated kernel is 31×31. (Best viewed on high-resolution display or refer to the supplemental material for better comparison.)

[7] D. Krishnan, T. Tay, and R. Fergus, "Blind deconvolution using a normalized sparsity measure," in *CVPR*, 2011, pp. 2657–2664.

[8] N. Joshi, R. Szeliski, and D. J. Kriegman, "PSF estimation using sharp edge prediction," in *CVPR*, 2008.

[9] T. S. Cho, S. Paris, B. K. P. Horn, and W. T. Freeman, "Blur kernel estimation using the radon transform," in *CVPR*, 2011, pp. 241–248.

[10] S. Cho and S. Lee, "Fast motion deblurring," *ACM Trans. Graph.*, vol. 28, no. 5, pp. 145, 2009.

[11] L. Xu and J. Jia, "Two-phase kernel estimation for robust motion deblurring," in *ECCV*, 2010, pp. 157–170.

[12] J. Pan, R. Liu, Z. Su, and X. Gu, "Kernel estimation from salient structure for robust motion deblurring," *Signal Processing: Image Commuincation*, vol. 28, no. 9, pp. 1156–1170, 2013.

[13] L. Sun, S. Cho, J. Wang, and J. Hays, "Edge-based blur kernel estimation using patch priors," in *ICCP*, 2013.

[14] L. Xu, S. Zheng, and J. Jia, "Unnatural l_0 sparse representation for natural image deblurring," in *CVPR*, 2013, pp. 1107–1114.

[15] J. Pan and Z. Su, "Fast ℓ^0-regularized kernel estimation for robust motion deblurring," *IEEE Signal Processing Letters*, vol. 20, no. 9, pp. 841–844, 2013.

[16] Z. Hu, J.-B. Huang, and M.-H. Yang, "Single image deblurring with adaptive dictionary learning," in *ICIP*, 2010, pp. 1169–1172.

[17] H. Zhang, J. Yang, Y. Zhang, and T. S. Huang, "Sparse representation based blind image deblurring," in *ICME*, 2011, pp. 1–6.

[18] J.-F. Cai, H. Ji, C. Liu, and Z. Shen, "Framelet based blind motion deblurring from a single image," *IEEE Transactions on Image Processing*, vol. 21, no. 2, pp. 562–572, 2012.

[19] M. Elad and M. Aharon, "Image denoising via sparse and redundant representations over learned dictionaries," *IEEE Transactions on Image Processing*, vol. 15, no. 12, pp. 3736–3745, 2006.

[20] A. Buades, B. Coll, and J.-M. Morel, "A non-local algorithm for image denoising," in *CVPR*, 2005, pp. 60–65.

[21] W. Dong, G. Shi, and X. Li, "Nonlocal image restoration with bilateral variance estimation: A low-rank approach," *IEEE Transactions on Image Processing*, vol. 22, no. 2, pp. 700–711, 2013.

[22] S. Wang, L. Zhang, and Y. Liang, "Nonlocal spectral prior model for low-level vision," in *ACCV*, 2012, pp. 231–244.

[23] S. Osher and L. I. Rudin, "Feature-oriented image enhancement using shock filters," *SIAM Journal on Numerical Analysis*, vol. 27, no. 4, pp. 919–940, 1990.

[24] J.-F. Cai, E. J. Candès, and Z. Shen, "A singular value thresholding algorithm for matrix completion," *SIAM Journal on Optimization*, vol. 20, no. 4, pp. 1956–1982, 2010.

[25] A. Levin, R. Fergus, F. Durand, and W. T. Freeman, "Image and depth from a conventional camera with a coded aperture," *ACM Trans. Graph.*, vol. 26, no. 3, pp. 70–78, 2007.

[26] L. Zhong, S. Cho, D. Metaxas, S. Paris, and J. Wang, "Handling noise in single image deblurring using directional filters," in *CVPR*, 2013, pp. 612–619.